RSC Advances

ROYAL SOCIETY OF CHEMISTRY

www.rsc.org/advances

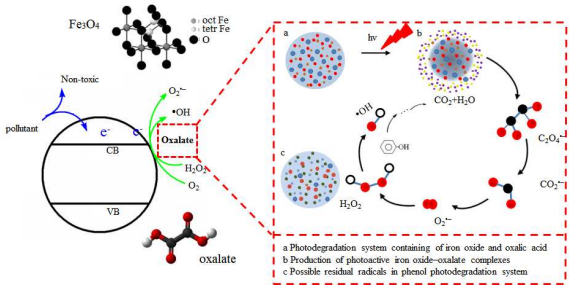

A novel approach for phenol removal using Fe_3O_4 nanoparticles and oxalate was proposed via a radical mechanism.

Photocatalytic degradation of phenol by the heterogeneous Fe_3O_4 nanoparticles and oxalate complex system

Piao Xu [a,b], Guangming Zeng [a,b,*], Danlian Huang [a,b,*], Liang Liu [a,b], Cui Lai [a,b], Ming Chen [a,b], Chen Zhang [a,b], Xiaoxiao He [a,b], Mingyong Lai [a,b], Yibin He [a,b]

[a] *College of Environmental Science and Engineering, Hunan University, Changsha 410082, PR China*

[b] *Key Laboratory of Environmental Biology and Pollution Control (Hunan University), Ministry of Education, Changsha 410082 ,PR China*

[*] Corresponding authors. College of Environmental Science and Engineering, Hunan University, Changsha 410082, China. Tel.: +86–731–88822754; fax: +86–731–88823701.

Email address: zgming@hnu.edu.cn (Guangming Zeng) and huangdanlian@hnu.edu.cn (Danlian Huang).

Abstract

A novel approach for the removal of phenol by an advanced oxidation process using Fe_3O_4 nanoparticles (NPs) and oxalate was proposed and investigated, and the influences of oxalate, Fe_3O_4 NPs and H_2O_2 dosage on the photodegradation of phenol were reported. No obvious difference is found between ultraviolet light and visible light exposure, confirmed potential photoactinic roles of Fe_3O_4 NPs in the presence of oxalate under visible light. Furthermore, relative highly dependence of oxalate depletion was observed, due to the initiation the formation of the Fe(III)-carboxylate complexes for photodegradation via a photo-Fenton-like system. Our results also demonstrated that the photodegradation of phenol occurred by a radical mechanism accompanied with the formation of $O_2^{\bullet-}$ and •OH radicals, which was further accelerated by the exogenous addition of H_2O_2. All reactions followed the pseudo-first-order reaction kinetics. The half-life ($t_{1/2}$) of Fe_3O_4-oxalate and Fe_3O_4-oxalate-H_2O_2 in the system showed higher efficiencies of photo-Fenton-like degradation routes for phenol. The photo-Fenton-like systems showed a relatively high catalytic ability (>99.9%) in the removal of phenol at low phenol concentrations below 50 mg L^{-1}, indicating its potential application in the treatment of low concentration wastewater. The results have demonstrated the feasibility of Fe_3O_4 NPs as potential heterogeneous photo-Fenton photocatalysts for organic contaminants decontamination in industrial wastewater.

1. Introduction

The efficient treatment of industrial wastewaters and contaminated drinking water sources has become of immediate importance that is facing with ever increasing population. Phenol and its derivates are among the most potential pollutants discharged from various industries, such as coal gasification, polymeric resin production, oil refining, coking plants, paper mill, herbicides and fungicides production.[1,2] Traditional methods such as solvent extraction, activated carbon adsorption, and common chemical oxidation often suffer from serious drawbacks including high cost or formation of hazardous by-products.[3,4] For example, biological decontamination by chlorination method might result in the formation of more toxic chlorinated compounds during the conversion process.

It has therefore gained much attention owing to the urgent need for a clean and comfortable environment. Heterogeneous photocatalysis is one of a promising method for the elimination of toxic and bio-resistant organic compounds by transforming them into innocuous species, which has been widely applied in the removal of organic pollutants in wastewater.[5-7] Various photocatalysts have been developed in the past decades, such as TiO_2, ZnO, CdS, WO_3, and ZnS, demonstrating its high efficiency in degradation of a wide range of refractory organic pollutants into innocuous carbon dioxide and water under UV irradiation.[8-10] However, limited efficiency and high cost in the use of irradiated energy limited the practical applications of heterogeneous photocatalysis. Considerable efforts have been made to enhance photocatalytic activity, such as decreasing photocatalyst size to increase surface area, combining

photocatalyst with some novel metal nanoparticles, and increasing hole concentration through doping.[11,12]

In recent years, the utilization of iron oxide nanoparticles (NPs) with novel properties and functions have been widely studied, due to their nano-range size, high surface area to volume ratios and superparamagnetism.[13-16] Most of iron oxides show semiconductor properties with narrow band gap (2.0–2.3 eV) and are photoactive under solar irradiation as photocatalysts absorbing visible light.[7,17,18] For example, Fe_2O_3 with band-gap of 2.2 eV is an interesting n-type semiconducting material and a suitable candidate for photodegradation under visible light condition. Moreover, iron oxide containing Fenton-like heterogeneous photocatalysis has been widely reported in many advanced oxidation processes, but the limited photocatalysis encountered frequently because of the electron–hole charge recombination at the oxide surface, as fast as within nanoseconds.[19,20] Accordingly, the mutual characterization of Fenton-reaction is the generation of hydroxyl radicals (•OH), a very powerful and active radical with high oxidative capacity (reduction potential of •OH E_0=2.8 V), which can react with almost all organic pollutants, yielding dehydrogenated or hydroxylated derivatives through a multistep process.[21] Thus, sufficient H_2O_2 have to be added to make the system efficient with •OH formation, resulting in the costly consumption of H_2O_2. As an alternative, a photo-Fenton-like system based on the iron oxides and polycarboxylic acids, such as oxalate, has been set up with the formation of •OH without the exogenous addition of H_2O_2.[22,23] However, the effect of oxalate on the heterogeneous photodegradation of phenol in

the presence of Fe_3O_4 nanoparticles has been scarcely studied.

In this study, we investigated phenol degradation by a Fe_3O_4-oxalate based photo-Fenton-like system. Parameters affecting photodegradation process such as pH, dosage of oxalate, Fe_3O_4 NPs and H_2O_2, and phenol concentration were examined. Special attention has been given to the mechanistic insight into photodegradation of phenol accompanied with the formation of reactive radicals. The results obtained in this study might shed some light on the possible route of phenol removal via photo-Fenton-like oxidation mechanism.

2. Experimental section

2.1. Chemicals

Iron chloride hexa-hydrate ($FeCl_3 \cdot 6H_2O$) and ferrous chloride tetra-hydrate $FeCl_2 \cdot 4H_2O$, 30% hydrogen peroxide, phenol and ethylene glycol were of analytical grade. Ultrapure water was used for the preparation of all the solutions throughout this study. Fe_3O_4 nanoparticles were prepared by coprecipitation of $FeCl_3 \cdot 6H_2O$ and $FeCl_2 \cdot 4H_2O$ in ammonia solution according to our previous study.[24]

2.2. Phenol photodegradation experiment

The phenol photodegradation experiment was implemented in a set of 250 mL conical flasks placed in a constant-temperature oscillator with a vibration rate of 150 rpm at 303 K. Different operation conditions, such as pH value, Fe_3O_4 NPs dosage, oxalate and hydrogen peroxide dosage and initial phenol concentration were investigated in the batch experiments. Solutions (100 mL) with the desired concentration of phenol

(10–300 mg L^{-1}) and the given oxalate concentrations (0–8.8 mM) at desired pH value (2.0–9.0) were fed into the reactor, and then Fe_3O_4 NPs (ranging from 0.1–4.0 g L^{-1}) and H_2O_2 (0–2.35 mM) were added simultaneously. The initial pH of the solution was adjusted to the desired value ranging from 2.0 to 9.0 by adding a small quantity of 0.1 M HCl or NaOH solution. All the experiments were carried out in triplicate and data presented were the mean values from these independent experiments.

2.3. Characterization of the Fe_3O_4 nanoparticles

The morphologies of Fe_3O_4 NPs were characterized by a field emission scanning electron microscopy (FESEM, JSM 6700F), equipped with energy disperse spectroscopy (EDS, EDAX genesis xm-2), after gold plating at an accelerating voltage of 20 kV for 30 s. The particle size of the Fe_3O_4 NPs was characterized by dynamic light scattering (DLS) using Zetasizer 3000HS (Malvern, UK) suspending in deionized water. The functional groups of Fe_3O_4 NPs were characterized by the corresponding Fourier transform infrared spectrophotometer (FTIR) spectra (Nicolet, Nexus-670) over the range 4000–400 cm^{-1}. The phase of prepared NPs was characterized by X ray powder diffraction (XRD, Rigaku Rotaflex D/Max-C) performed by a monochromatized X-ray beam with nickel–filtered CuK_α radiation.

2.4. Analytical procedures

At the given time intervals, the analytical samples were taken from the suspension filtered with a 0.45 μm Millipore filter and used for selected index detection immediately. The concentration of phenol was determined by spectrophotometric

method at wavelength of 510 nm based on a chromogenic reaction between phenol and 4-aminoantipyrine in the presence of potassium ferricyanide via UV-vis spectrophotometer (UV-2550, Shimadzu).

Oxalate concentration residual in the solution was analyzed by HPLC (Agilent 1100) equipped with UV-vis variable wavelength detector (VWD) and reversed-phase C18 column. Phosphoric acid (0.15% v/v) was used as the mobile phase at a flow rate of 0.5 mL min^{-1} with the constant detection wave length at 210 nm. 10 μL of aqueous standard samples was injected into the liquid chromatograph. The column was maintained at 30°C.[25] Total Fe concentration was analyzed by atomic absorption spectrometry and ferrous ion (Fe^{2+}) concentration was analyzed by the ferrozine method as described by Paipa et al..[26] The production of superoxide anion ($O_2^{\bullet-}$) was measured with a Shimadzu 2550 UV–vis spectrophotometer at 530 nm according to our previous study.[27] The variation of hydroxyl radicals (•OH) produced during the photocatalytic reactions was characterized as the absorbance variation at 532 nm which detected in terms of thiobarbituric acid (TBA) method.[27]

3. Results and discussion

3.1. Characterization of Fe_3O_4 nanoparticles

Fig. 1a and Fig. 1b show SEM images of the Fe_3O_4 NPs, and it can be seen that the Fe_3O_4 NPs were distributed evenly with the homogeneity dimensional size. Meanwhile, EDS results shows in Fig. 1c demonstrate the enrichment of Fe and O element in Fe_3O_4 NPs. Fig. 1d shows that the size distribution of the sample is

comparatively narrow, concentrated at diameters of approximately 12–20 nm. Most importantly, the prepared Fe_3O_4 NPs can be removed conveniently with an external magnet. Fig. 1e shows a digital photograph of the phenol solution with equally dispersed Fe_3O_4 NPs before and after magnetic separation using an external magnetic field. It is apparent that easy, fast separation of the Fe_3O_4 NPs can be realized during the experiments. Meanwhile, FTIR spectra of Fe_3O_4 NPs depicted two strong absorption bands at around 437 and 588 cm^{-1}, which demonstrated by vibrations of Fe−O bonds of Fe_3O_4 NPs. Meanwhile, the absorption bands at 3403 cm^{-1} might be ascribed to the presence of O−H at the surface of Fe_3O_4 NPs (Fig. 2a). Characteristic peaks at 2θ=31.4º, 35.4º and 55.2º are observed in Fig. 2b, which can be assigned to magnetite.

3.2. Effect of pH on phenol photodegradation

The role of pH on the phenol removal was studied in the pH range 2.0–9.0 at phenol concentration of 100 mg L^{-1} (Fig. 3). Obviously, different tendencies are observed in various systems. For example, Fe_3O_4 NPs showed the highest removal efficiency at pH 5.0, while at pH 6.0 in Fe_3O_4-H_2O_2 system (0.1 mM). At the absence of oxalate, alkaline range is expected to favor the formation of •OH radicals in Fe_3O_4-H_2O_2 system thus enhance the degradation ability.[28] However, for a solution initially containing 100 mg L^{-1} phenol, only about 6% of phenol is degraded by Fe_3O_4 NPs without the addition of oxalate and H_2O_2 at pH 2.0–3.0. Results indicated that adsorption mechanism played limited roles in phenol removal process.

Obviously, the initial pH value tends to be a very important factor affecting the photo Fenton-like processes. Distinct enhancement of phenol removal is found in the acidic region than in the alkaline region in both Fe_3O_4-oxalate (2.0 mM) and Fe_3O_4-oxalate-H_2O_2 systems. The maximum degradation occurred in the acidic pH range at 2.0–3.0, based on the fact that acid range could favor for the formation of $FeIII(C_2O4)_2^-$ and $FeIII(C_2O_4)_3^{3-}$ initiating a series of photochemical reactions in Fe_3O_4-oxalate and Fe_3O_4-oxalate-H_2O_2 systems.[29] In addition, phenol has a hydroxyl group in its molecular structure, which is negatively charged, the acidic solution favors adsorption of phenol onto the Fe_3O_4 surface, leading to the improvement of the degradation efficiency. Sharp depletion of phenol degradation above pH 4.0 implies that the operating conditions are at acid pH range, mainly due to the inactive formation of photoactive groups with the increasing pH. When the pH value increased to about 4.0–5.0, Fe(III)–oxalate species were mainly $FeIII(C_2O_4)^+$, which was low photoactive.[30] When the pH value was up to 6.0, the Fe^{3+} and Fe^{2+} almost cannot exist in the solution and the predominant Fe(III) and Fe(II) species were Fe(II)–OH and Fe(III)–OH as the precipitate, which might hardly be photoactive. Simultaneously, as pH was raised from 2.0 to 9.0, the phenol degradation efficiency decrease from 89.52% to 25.37% in Fe_3O_4-oxalate system. Additionally, H_2O_2 as an oxidant was also applied to phenol degradation, and the degradation efficiency of phenol in the presence of neat oxalate, oxalate-H_2O_2, $FeCl_2$-oxalate-H_2O_2 and $FeCl_3$-$FeCl_2$-oxalate-H_2O_2 systems were also investigate to compare with the degradation ability of conventional methods (Table 1). As a result, relative low

188 removal efficiency was found in oxalate, H_2O_2 and oxalate-H_2O_2 system. However,
189 the phenol degradation promoted in $FeCl_2$-oxalate-H_2O_2 and
190 $FeCl_3$-$FeCl_2$-oxalate-H_2O_2 system, mainly due to the potential occurrence of
191 photocatalytic reaction between Fe^{2+} and oxalate in the presence of H_2O_2.
192 Consequently, it was apparent that Fe_3O_4-oxalate-H_2O_2 system showed the
193 predominant degradation ability to phenol in the all tested degradation systems.

194 **3.3. Effect of oxalate concentration on phenol photodegradation**

195 Fig. 4 shows the effect of oxalate concentration (0–8.8 mM) on phenol
196 photodegradation under ultraviolet light and visible light, respectively. It is apparent
197 that no obvious difference is found between ultraviolet light and visible light exposure,
198 which confirmed potential photocatalytic roles of Fe_3O_4 NPs under solar irradiation in
199 the presence of oxalate. Visible light is chosen as light source in the following study.
200 Apparently, phenol removal was greatly promoted by the addition of oxalate from
201 0–2.2 mM. In the absence of oxalate, Fe_3O_4 NPs mainly acted as adsorbents and the
202 photochemical transformation rate for organic pollutants on the surface of Fe_3O_4 NPs
203 might be negligible under visible light.[31] While in the presence of oxalate, the
204 heterogeneous Fe_3O_4–oxalate complex formed and a photo-Fenton-like system was
205 set up, exhibiting a strong ligand-to-metal charge transformation ability.[31] In this
206 heterogeneous photo-Fenton-like system, Fe_3O_4 NPs mainly acted as a photocatalyst,
207 while oxalic acid could be excited to generate electron-hole pairs.[32,33] In previous
208 work conducted by Balmer and Sulzberger,[34] high photoactive groups $Fe(C_2O_4)_2^-$ and
209 $Fe(C_2O_4)_3^{3-}$ have been detected in the iron oxide-oxalate system. This is the reason

why photodegradation efficiency is enhanced greatly in the presence of oxalate. However, excessive existence oxalate inhibited the photodegradation process. First of all, excessive oxalate would lead to the formation of a large amount of Fe^{3+}, which would inhibit the formation of H_2O_2. In addition, excessive oxalate would occupy the adsorbed sites on the surface of Fe_3O_4 NPs and react competitively for •OH.[29] Obviously, an optimal amount of oxalate achieving the best performance of the photodegradation of phenol was at the value of 2.2 mM.

From Fig. 4b, it was obviously that depletion of oxalate occurred during phenol degradation process, which was consistent with the previous hypothesis that oxalate participated in phenol photodegradation via a photo-Fenton like system. Oxalate was strongly complexed with the Fe_3O_4 NPs with the formation of photoactive groups accelerating phenol photodegradation, contributing to the oxalate depletion. Significant correlations have been observed between oxalate depletion and phenol degradation efficiency, especially at the dietary range of oxalate concentration below 1.1 mM (Fig. 4b), based on the fact that oxalate participated in photo-Fenton-like system via a series of reaction for the formation of reactive radicals.

3.4. Possible mechanism involved in the photodegradation of phenol

Accordingly, the photochemical transformation could be improved when Fe_3O_4 NPs and oxalate set up a photo Fenton-like system due to the formation of Fe(III)-carboxylate complexes.[19,20,26] Firstly, oxalate is adsorbed by Fe_3O_4 NPs to form Fe_3O_4-oxalate complexes including $[FeIII(C_2O_4)_n]^{(2n-3)}$ or $[FeII(C_2O_4)_{n-1}]^{4-2n}$ (Eqs. 1–3), which are much more photoactive than the other Fe^{3+} species, with the

generation of oxalate radical $C_2O_4^{\bullet-}$ (Eq. 3). Then, oxygen trapped the electron from $C_2O_4^{\bullet-}$ and a rapid decarboxylation of $C_2O_4^{\bullet-}$ followed, with the formation of $O_2^{\bullet-}$ (Eq. 5). Under the acidic pH range, the formed $O_2^{\bullet-}$, further formed in •OOH, via capturing a proton, which could further reacted with Fe^{2+} contributing to the generation of H_2O_2 (Eqs. 6–7). H_2O_2 further reacts with Fe^{2+} to form •OH (Eq. 8), which generated in their redox-oxidize transformation process accompanied with the production and consumption of H_2O_2, as described below, played a key role in the photodegradation course. Thereafter, organic pollutants will be attacked by •OH and mineralized efficiently in phenol photodegradation system. The illustration of the photodegradation mechanism is shown in Fig. 5.

$$\text{Iron oxide} + nH_2C_2O_4 \leftrightarrow [\equiv Fe(C_2O_4)_n]^{(2n-3)-} \quad (1)$$

$$[\equiv Fe(C_2O_4)_n]^{(2n-3)-} + hv \rightarrow Fe(C_2O_4)_2^{2-} \text{ or } (\equiv Fe(C_2O_4)_2^{2-}) + CO_2^{\bullet-} \quad (2)$$

$$[Fe^{III}(C_2O_4)_n]^{(2n-3)-} + hv \rightarrow [Fe^{II}(C_2O_4)_{n-1}]^{4-2n} + C_2O_4^{\bullet-} \quad (3)$$

$$C_2O_4^{\bullet-} \rightarrow CO_2 + CO_2^{\bullet-} \quad (4)$$

$$C_2O_4^{\bullet-} + O_2 \rightarrow CO_2 + O_2^{\bullet-} \quad (5)$$

$$Fe^{3+} + O_2^{\bullet-} \rightarrow Fe^{2+} + O_2 \quad (6)$$

$$O_2^{\bullet-} + nH^+ + Fe^{2+} \rightarrow Fe^{3+} + H_2O_2 \quad (7)$$

$$Fe^{2+} + H_2O_2 \rightarrow Fe^{3+} + OH^- + \bullet OH \quad (8)$$

$$\bullet OH + HC_2O_4^{\bullet-} \rightarrow CO_2 + CO_2^{\bullet-} + H_2O \quad (9)$$

In order to better understand the photodegradation mechanism, the changes in $O_2^{\bullet-}$ and •OH during the course of the reaction were measured to verify the formation and dependence of $O_2^{\bullet-}$ and •OH radicals on the phenol photodegradation (Fig. 6). For

both Fe_3O_4-oxalate and Fe_3O_4-oxalate-H_2O_2 system, the formation of $O_2^{\bullet-}$ and •OH radicals at the initial 5 min has been found, and the addition of exogenous H_2O_2 promoted the production of $O_2^{\bullet-}$ and •OH. However, as the mobility and reactivity of radicals, it can be speculated that $O_2^{\bullet-}$ and •OH radicals, immediately after formation, leave the surface of Fe_3O_4 NPs and participated in the photodegradation reaction as shown in the above. As a result, a distinct depletion in both $O_2^{\bullet-}$ and •OH occurred at the end of the photodegradation process (Fig. 6).

3.5. Dynamic photodegradation of phenol

Fig. 7 shows the dynamics of phenol photodegradation by Fe_3O_4 NPs, Fe_3O_4-H_2O_2, Fe_3O_4-oxalate and Fe_3O_4-oxalate-H_2O_2 systems. It was found that, the concentration of the phenol remained almost unchanged after 180 min in the presence of Fe_3O_4 NPs. The observations demonstrated that the photocatalytic experiments occurred in a pure photocatalytic regime where Fe_3O_4 derived adsorption process could be neglected.

Significantly enhanced degradation rates of phenol were observed when oxalate was added into Fe_3O_4 nanoparticles. The behavior of phenol degradation by Fe_3O_4-oxalate and Fe_3O_4-oxalate-H_2O_2 was quite different from that by Fe_3O_4 or Fe_3O_4-H_2O_2; for the former reaction occurred similar to Fenton chemistry, through the participation of •OH in activating phenol degradation via Fenton-like oxidation process. One of the key stages in Fenton's processes is the generation of the oxidizing species, such as •OH, by initiating of H_2O_2 decomposition.[25] The rate constants corresponding to •OH attack were taken from literature values or assigned a generic value in the range of (5×10^9)–(1×10^8) depending on the analogies between the

compounds considered and other species whose kinetic constants are known.[25] Iron oxides and oxalate could trigger the Fenton-like oxidation process without additional H_2O_2 in the case of the intermediate role of oxalate generating •OH radicals. Almost 96% of phenol is degraded after 180 min in described photocatalyst system, exhibiting efficient photocatalytic activity under visible-light irradiation.

Phenol concentration versus the reaction time was further conducted by the equation of pseudo-first-order kinetics $\ln(C/C_0)=-kt$, where C_0 and C are the phenol concentrations in solution at times 0 and t, respectively, and k is the pseudo-first-order rate constant. Additionally, initial degradation rate is expressed as the degradation rate at the beginning of irradiation ($r_{in}=kC_0$). The calculated values of the initial rate were used for a comparison of the efficiency of the photodegradation process under different reaction conditions. The data adequately fitted the pseudo-first order model in Fe_3O_4-oxalate and Fe_3O_4-oxalate-H_2O_2 system, with high correlation coefficients of 0.9655 and 0.9852, respectively (Fig. 7b). Pseudo-first-order rate constants were estimated as given in Table 2. The initial oxidation rate was accelerated from 0.03 mg L^{-1} min^{-1} to 1.83 mg L^{-1} min^{-1} by comparison between Fe_3O_4 NPs and Fe_3O_4-oxalate systems. Furthermore, the addition of H_2O_2 into Fe_3O_4-oxalate systems further accelerated the rate of phenol photodegradation, due to the fact that the exogenous H_2O_2 would promoted the formation of •OH radicals. Meanwhile, the value of half-life, that is, the time required to decrease the concentration of the reactant to half the amount present before the reaction, was also presented in Table 2. It is apparent that half time of Fe_3O_4-oxalate and Fe_3O_4-oxalate-H_2O_2 systems is much smaller than

298 those Fe_3O_4 nanoparticles.

299 **3.6. Effect of Fe_3O_4 nanoparticles on phenol photodegradation**

300 To test the effect of Fe_3O_4 nanoparticles on phenol degradation, the experiments were
301 carried out in the suspension with an initial concentration of 50 mg L^{-1} phenol at pH
302 2.0 (Fig. 8). Fe_3O_4 NPs applied at the whole concentrations improved phenol removal,
303 but the improvements were not closely proportional to the Fe_3O_4 NPs concentration
304 elevation. Fig. 8 demonstrates that the increase of Fe_3O_4 NPs at the range of 0.1–1.0 g
305 L^{-1} resulted in an elevation in phenol photodegradation, thereafter tend to be
306 stationary in the presence of 2.0 to 4.0 g L^{-1} Fe_3O_4 NPs. When sufficient
307 photocatalysts are available, the reaction proceeds rapidly to a decrease in phenol,
308 ensuring complete degradation of phenol. Fig. 7 also shows the iron species, Fe(II)
309 and Fe(III), in the solution after 3 h of photodegradation in the presence of a series of
310 concentration of Fe_3O_4 NPs. Apparently, the concentration of Fe(II) and Fe(III)
311 depended strongly on the initial Fe_3O_4 NPs. A higher Fe_3O_4 dosage contributed to a
312 higher concentration of Fe(II) and Fe(III) during phenol photodegradation process.

313 **3.7. Effect of H_2O_2 on phenol photodegradation**

314 It is widely reported that the involution of H_2O_2 is a critical issue of the Fenton and
315 related oxidation processes. The effect of the use of H_2O_2 on the phenol degradation
316 can be clearly observed in Fig. 9. The efficiency of the methods in terms of total
317 phenol removal reveals that the addition of H_2O_2 to the Fe_3O_4-oxalate system
318 enhances the organics conversion. By considering the evolution profiles of individual

phenols, higher induction of phenol removal was observed when applying the promoted photocatalytic process; however, the continuously supply of H_2O_2 showed insignificant effect on phenol degradation, once a sufficient amount of radicals has been generated.

As inferred from Fig. 9, there is an optimum concentration of H_2O_2. The highest efficiency of phenol degradation was obtained with the addition of 0.236 mM H_2O_2, at the value of 98.70%. The auxo-action role of H_2O_2 involved in phenol degradation might occur in two possible pathways. On the one hand, H_2O_2 can directly react with the parent compounds starting a chain mechanism in the presence of oxygen, on the other hand (most probable), H_2O_2 might decompose into •OH via the Fenton reaction. According to above equations, photolysis of Fe_3O_4-oxalate complexes forms H_2O_2, endowing the acceptable degradation efficiency at the absence of H_2O_2 in Fe_3O_4-oxalate photocatalysis via various pathways, for instance, electron trapping, thermal decomposition, reaction with superoxide radicals, moreover, the phenol conversion is enhanced by the participation of H_2O_2. The increase of the photocatalytic rates with the exogenous addition of H_2O_2 can be attributed to the thermodynamically more favorable formation of •OH in the case of sufficient H_2O_2 supplying. From the theoretical point of view, increasing the amount of H_2O_2 would eventually lead to a higher •OH generation through electron trapping or homogeneous scission. However, excessive H_2O_2 might lead to a decrease in phenol degradation. Even, at high concentrations, H_2O_2 might become a scavenger of valence band holes and •OH (Eqs. 10-11). Additionally, it has been reported that an excess of H_2O_2

concentration also involves an increase in its inefficient decomposition to yield oxygen and water instead of hydroxyl radicals [25].

$$H_2O_2+2h_{VB}^{+}\rightarrow O_2+2H^{+} \quad (10)$$

$$H_2O_2+ \bullet OH\rightarrow HO_2\bullet+H_2O \quad (11)$$

3.8. Effect of initial phenol concentration

Fig. 10 illustrates the photodegradation efficiency at various initial phenol concentrations. Slight increases in phenol photodegradation were observed by comparison with the Fe_3O_4-oxalate and Fe_3O_4-oxalate-H_2O_2 systems. It was found that the phenol removal efficiency almost remained stable of 99.9% when C_0 was less than 20 mg L^{-1}, and the highest phenol removal efficiency of 99.96% was obtained when C_0 was 20 mg L^{-1} degraded by Fe_3O_4-oxalate-H_2O_2 system. With the continuous increase of phenol, a slight decrease occurred, based on the fact that the photodegradation process may be controlled by the limited numbers of surface sites of the photocatalyst with the excess phenol concentrations. The present results indicated that photocatalytic oxidation process is rather promising at low phenol concentrations, which is considered to be of a great importance in industrial applications.

4. Conclusions

In this work, Fe_3O_4-oxalate based photo-Fenton-like system performed photodegradation of phenol was studied. The Fe_3O_4 NPs were prepared with the homogeneity dimensional size concentrated at diameters of approximately 12–20 nm. Photodegradation efficiency was highly pH dependent and decreased with an increase of pH in the range of 2.0–9.0. Independence of oxalate is proven to enhance

the photocatalytic activity of the Fe_3O_4 NPs in the case of initiation of H_2O_2 which triggered the $O_2^{\bullet-}$ formation and •OH generation via Fenton reaction. Equilibrium data were well fitted by Pseudo-first-order kinetic models. Moreover, exogenous addition of H_2O_2 also enhanced the photodegradation of phenol, with the promoted formation of $O_2^{\bullet-}$ and •OH. The optimal photodegradation condition occurred at pH 2.0 and at the concentration of 2.2 mM oxalate and 0.236 mM H_2O_2. Under the optimal conditions, 99.92% and 97.61% of phenol were removed at phenol concentration of 10 mg L^{-1} and 100 mg L^{-1}, respectively. In conclusion, it appears that iron oxide nanomaterials are suitable for wastewater treatment through photodegradation and that more investigations are needed to design and optimize an industrial continuous process for phenol removal from wastewater.

Acknowledgements

The study was financially supported by the National Natural Science Foundation of China (51378190, 51039001, 51278176), the Hunan Provincial Innovation Foundation For Postgraduate (CX2013B152, CX2012B137), the Zhejiang Provincial Key Laboratory of solid Waste Treatment and Recycling open fun (SWTR-2012-07), the Environmental Protection Technology Research Program of Hunan (2007185), the New Century Excellent Talents in University (NCET-13-0186) and the Program for Changjiang Scholars and Innovative Research Team in University (IRT-13R17).

References

1 R.L. Qiu, D.D. Zhang, Z.H. Diao, X.F. Huang, C. He, J.L. Morel and Y. Xiong,

384 *Water Res.,* 2012, 46, 2299-2306.

385 2 G.M. Zeng, M. Chen and Z.T. Zeng, *Nature*, 2013, **499**, 154.

386 3 S. Esplugas, J. Gimenez, S. Contreras, E. Pascual and M. Rodríguez, *Water Res.*,

387 2002, **36**, 1034-1042.

388 4 M.A. Lazar and W.A. Daoud, *RSC Adv.*, 2013,**3**, 4130-4140 .

389 5 Y. Li, J. Wang, H. Yao, L. Dang and Z. Li, *J. Mol. Catal. A: Chem.*, 2011, **334**,

390 116-122.

391 6 M. Pera-Titus, V. García-Molina, M.A. Banos, J. Giménez and S. Esplugas, *Appl.*

392 *Catal. B: Environ.*, 2004, **47**, 219-256.

393 7 W. Jiang, Q. Cai, W. Xu, M. Yang, Y. Cai, D.D. Dionysiou and K.E. O'Shea,

394 *Environ. Sci. Technol.*, 2014, DOI: 10.1021/es405804m.

395 8 P. Xu, G.M. Zeng, D.L. Huang, C.L. Feng, S. Hu, M.H. Zhao, C. Lai, Z. Wei, C.

396 Huang and G.X. Xie, *Sci. Total Environ.*, 2012, **424**, 1-10.

397 9 T.J. Liu, Q.W. and P. Jiang, *RSC Adv.*, 2013, **3**, 12662-12670.

398 10 M. Yasui, K. Katagiri, S. Yamanaka and K. Inumaru, *RSC Adv.*, 2012, **2**,

399 11132-11137.

400 11 D. Vione, C. Minero, V. Maurino, M.E. Carlotti, T. Picatonotto and E. Pelizzetti,

401 *Appl. Catal. B: Environ.*, 2005, **58**, 79-88.

402 12 X.W. Zhang and L.C. Lei, *Appl. Surf. Sci.* 2008, **254**, 2406-2412.

403 13 S.A.C. Carabineiro, N. Bogdanchikova, P. B. Tavares and J.L. Figueiredo, *RSC*

404 *Adv.*, 2012,**2**, 2957-2965.

405 14 M. Niu, F. Huang, L. Cui, P. Huang, Y. Yu and Y. Wang, *ACS Nano*, 2010, **4**,

406 681-688.

407 15 P. Xu, G.M. Zeng, D.L. Huang, C. Lai, M.H. Zhao, Z. Wei, N.J. Li, C. Huang and

408 G.X. Xie, *Chem. Eng. J.*, 2012, **203**, 423-431.

409 16 J. L. Gong, B. Wang, G. M. Zeng, C.P. Yang, C.G. Niu, Q.Y. Niu, W.J. Zhou and Y.

410 Liang, *J. Hazard. Mater.*, 2009, **164**, 1517-1522.

411 17 J.K. Leland and A.J. Bard, *J. Phys. Chem.*, 1987, **91**, 5076-5083.

412 18 X.H. Feng, H.J. Guo, K. Patel, H. Zhou and X. Lou, *Chem. Eng. J.*, 2014, **244**,

413 327-334

414 19 G. Rothenberger, J. Moser, M. Graetzel, N. Serpone and D.K. Sharma, *J. Am.*

415 *Chem. Soc.*, 1985, **107**, 8054-8059.

416 20 X. Zhong, S. Royer, H. Zhang, Q. Huang, L. Xiang, S. Valange and J. Barrault, *Sep.*

417 *Purif. Technol.*, 2011, **80**, 163-171.

418 21 E. Bizani, K. Fytianos, I. Poulios and V. Tsiridis, *J. Hazard. Mater.*, 2006, **136**,

419 85-94.

420 22 Y. Zuo and J. Hoigne, *Environ. Sci. Technol.*, 1992, **26**, 1014-1022.

421 23 B.M. Voelker, F.M. Morel and B. Sulzberger, *Environ. Sci. Technol.*, 1997, **31**,

422 1004-1011.

423 24 P. Xu, G. Zeng, D. Huang, S. Hu, C. Feng, C. Lai, M. Zhao, C. Huang, N. Li and Z.

424 Wei, *Colloid. Surface. A: Physicochem. Eng. Aspects*, 2013, **419**, 147-155.

425 25 N.J. Li, G.M. Zeng, D.L. Huang, S. Hu, C.L. Feng, M.H. Zhao, C. Lai, C. Huang,

426 Z. Wei and G.X. Xie, *Bioresour. Technol.*, 2011, **102**, 8137-8142.

427 26 C. Paipa, E. Poblete and M.I. Toral, *Miner. Eng.*, 2006, **19**, 1465-1468.

27 M. Cheng, G.M. Zeng, D.L. Huang, L. Liu, M.H. Zhao, C. Lai, C. Huang, Z. Wei, N.J. Li, P. Xu, C. Zhang, F.L. Li and Y. Leng, *Biochem. Eng. J.*, 2014, **84**, 9-15.

28 F.J. Rivas, J. Frades, M.A. Alonso, C. Montoya and J. Monteagudo, *J. Agr. Food Chem.*, 2005, **53**, 10097-10104.

29 J. Lei, C.S. Liu, F.B. Li, X.M. Li, S.G. Zhou, T.X. Liu, M.H. Gu and Q.T. Wu, *J. Hazard. Mater.*, 2006, **137**, 1016-1024.

30 N. Quici, M.E. Morgada, G. Piperata, P. Babay, R.T. Gettar and M.I. Litter, *Catal. Today*, 2005, **101**, 253–260.

31 F.B. Li, J.J. Chen, C.S. Liu, J. Dong and T.X. Liu, *Biol. Fert. Soils*, 2006, **42**, 409-417.

32 J.K. Leland and A.J. Bard, *J. Chem. Phys.*, 1987, **91**, 5076-5083.

33 C. Siffert and B. Sulzberger, *Langmuir*, 1991, **7**, 1627-1634.

34 C. Liu, F. Li, X. Li, G. Zhang and Y. Kuang, *J. Mol. Catal. A: Chem.*, 2006, **252**, 40-48.

Figure legends

Fig. 1. Characterization of Fe_3O_4 nanaopaticles via SEM images (a and b), EDS image (c), Particle Size analyzer (d) and magnetic seperation image (e).

Fig. 2. Characterization of Fe_3O_4 nanaopaticles via FTIR (a) and XRD (b).

Fig. 3. Photodegradation behavior of phenol at different pH in various Fe_3O_4-based degradation systems (time 4 h, Fe_3O_4 NPs 0.5 g L^{-1}, initial phenol concentration 100 mg L^{-1}).

Fig. 4. (a) Phenol degradation in Fe_3O_4 NPs-oxalate system with various dosages of oxalate under ultraviolet (solid) and visible light (hollow); (b) Correlation between oxalate depletion and phenol photodegradation (pH 2.0, Fe_3O_4 NPs 1.0 g L^{-1}, time 4 h, initial phenol concentration 100 mg L^{-1}).

Fig. 5. Schematic diagram of photodegradation mechanism of Fe_3O_4-oxalate system under visible light irradiation.

Fig. 6. Variation of $O_2^{\bullet-}$ and •OH radicals in Fe_3O_4-oxalate and Fe_3O_4-oxalate-H_2O_2 systems at the initial and end of the phenol photodegradation process (pH 2.0, Fe_3O_4 NPs 1.0 g L^{-1}, initial phenol concentration 100 mg L^{-1}, H_2O_2 dosage 0 and 0.118 mM, respectively).

Fig. 7. (a) Time course of phenol degradation in a series of Fe_3O_4 based systems and (b) Pseudo-first-order kinetics of phenol degradation (pH 2.0, oxalate 2.2 mM, time 3 h, initial phenol concentration 100 mg L^{-1}).

Fig. 8. Fe_3O_4 NPs dependent phenol degradation in Fe_3O_4-oxalate system with various dosages of Fe_3O_4 NPs and speciation of Fe(II) and Fe(III) in the solution in the

464 photodegradation process (pH 2.0, oxalate 2.2 mM, time 3 h, initial phenol
465 concentration 100 mg L^{-1}) .

466 **Fig. 9.** H_2O_2 dependent phenol degradation and residual H_2O_2 concentration in Fe_3O_4
467 NPs-oxalate system with various dosages of H_2O_2 (pH 2.0, Fe_3O_4 NPs 1.0 g L^{-1},
468 oxalate 2.2 mM, time 3 h, initial phenol concentration 100 mg L^{-1}).

469 **Fig. 10.** Concentration-dependent phenol degradation and residual phenol
470 concentrations in the presence of Fe_3O_4-oxalate and Fe_3O_4-oxalate-H_2O_2 system (pH
471 2.0, Fe_3O_4 NPs 1.0 g L^{-1}, oxalate 2.2 mM, time 3 h, H_2O_2 0 and 0.236 mM,
472 respectively).

473

474 **Table Legends**

475 **Table 1** Phenol degradation efficiency in various oxalate and H_2O_2 containing systems

476 **Table 2** Pseudo-first-order kinetic constants for the photodegradation of phenol

477

478 **Table 1** Phenol degradation efficiency in various oxalate and H_2O_2 containing

479 systems

	oxalate	H_2O_2	oxalate-H_2O_2	$FeCl_2$-oxalate-H_2O_2	$FeCl_3$-$FeCl_2$-oxalate-H_2O_2
pH 3	6.30%	20.35%	23.32%	58.98%	57.42%
pH 5	5.21%	25.76%	29.39%	64.91%	63.52%

480

481 **Table 2** Pseudo-first-order kinetic constants for the photodegradation of phenol

Process	Rate constant k, min^{-1}	Initial oxidation rate (mg L^{-1} min)	$t_{1/2}$ (h)	R^2
Fe_3O_4	0.0003	0.03	38.51	0.8141
Fe_3O_4-H_2O_2	0.0017	0.17	6.80	0.8529
Fe_3O_4-oxalate	0.0183	1.83	0.63	0.9655
Fe_3O_4-oxalate -H_2O_2	0.0190	1.90	0.61	0.9852

482

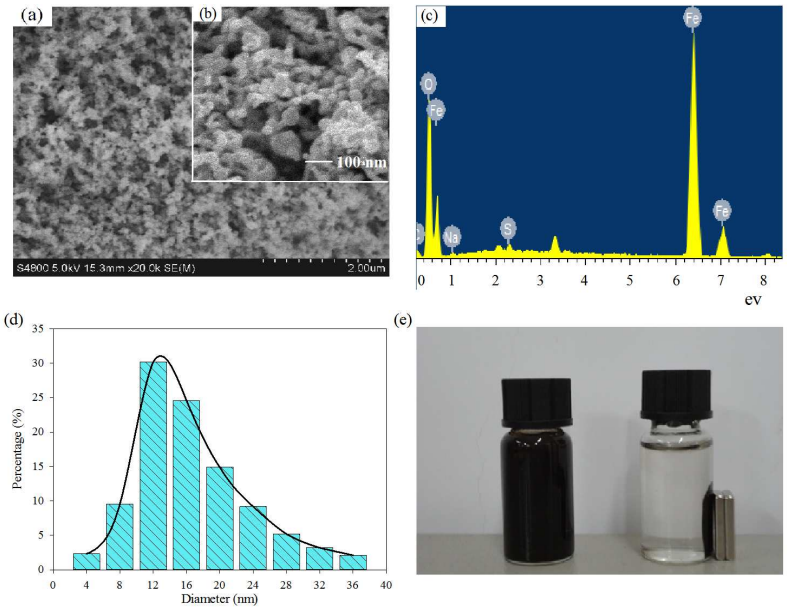

Fig. 1

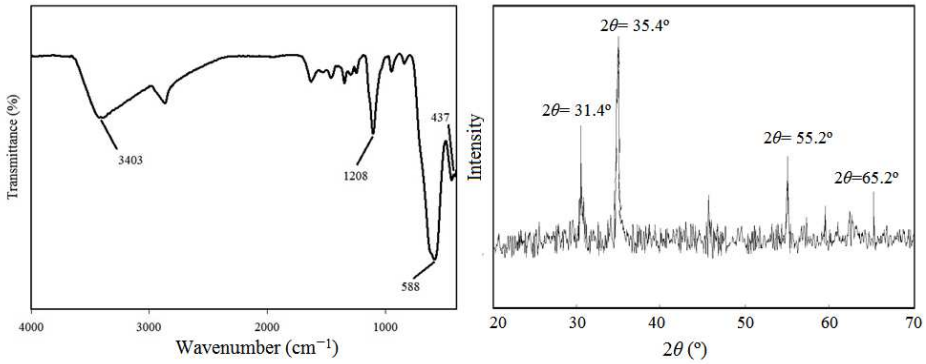

Fig. 2

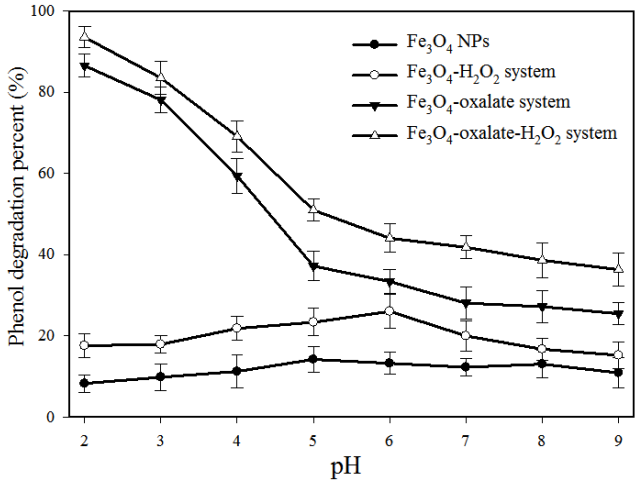

Fig. 3

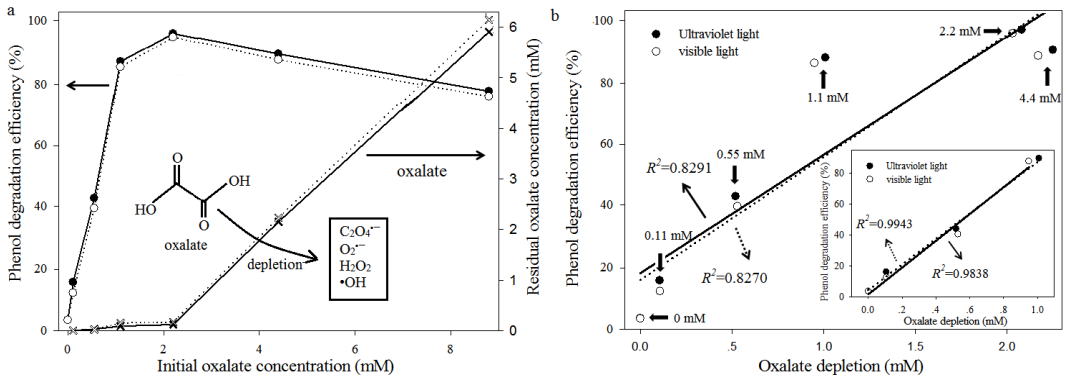

Fig. 4

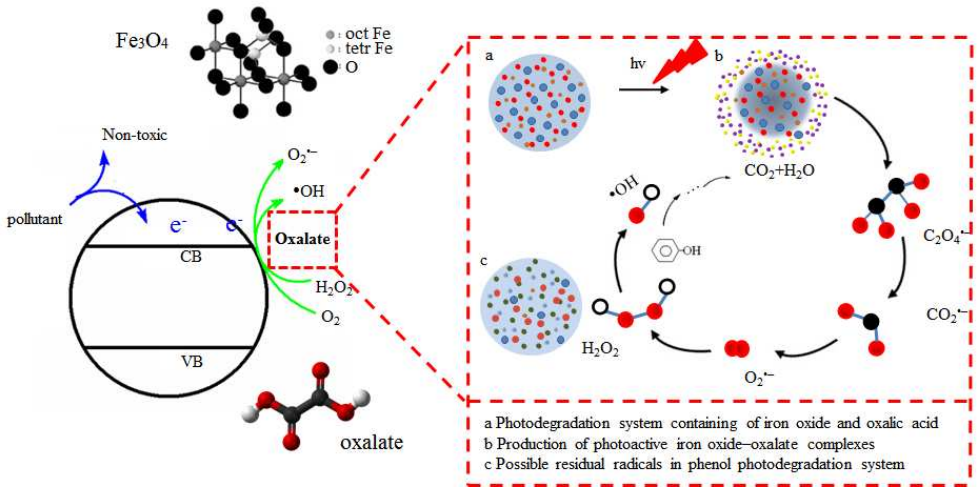

Fig. 5

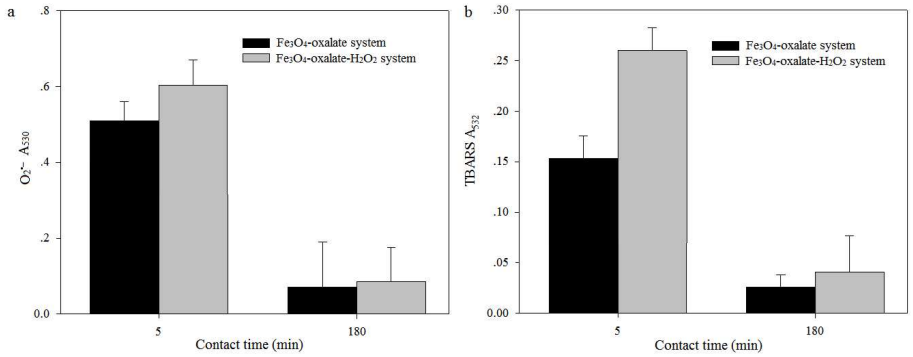

Fig. 6

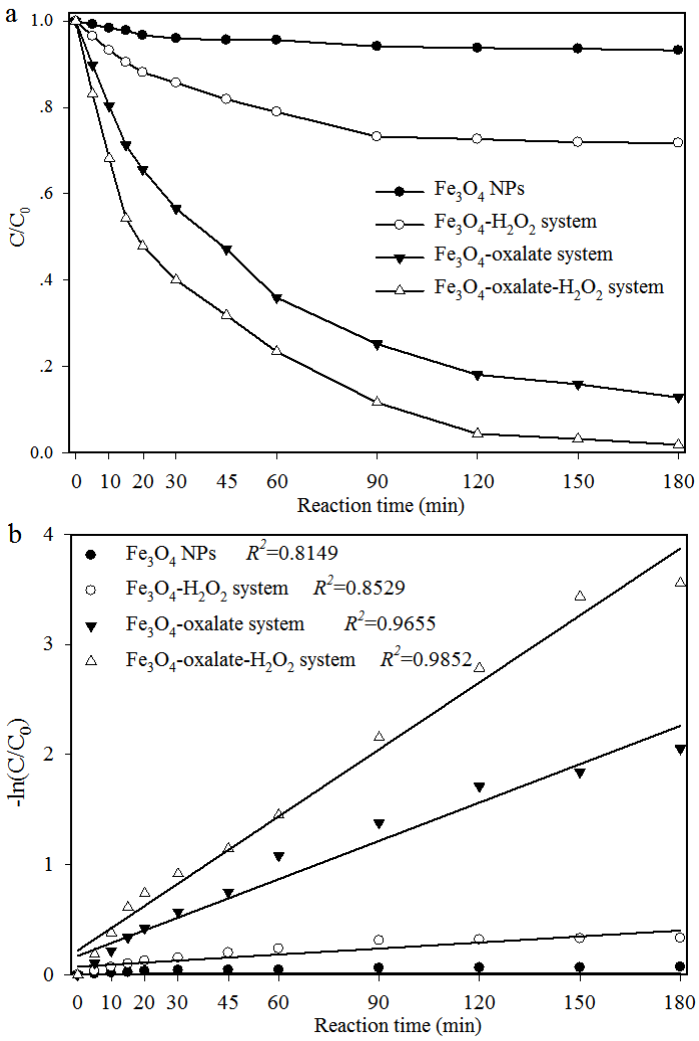

Fig. 7

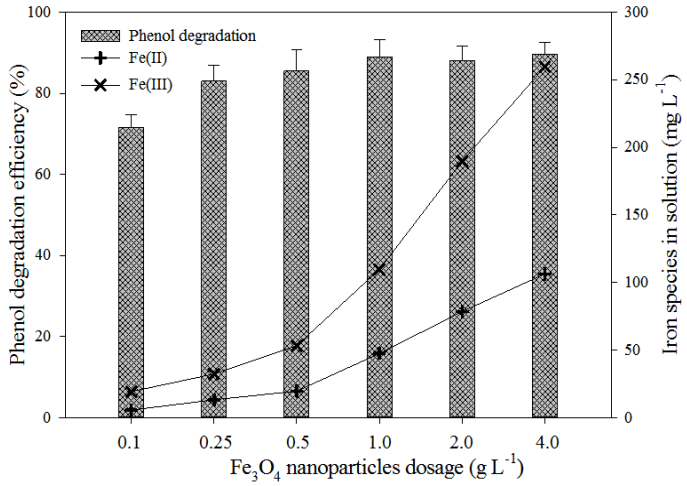

Fig. 8

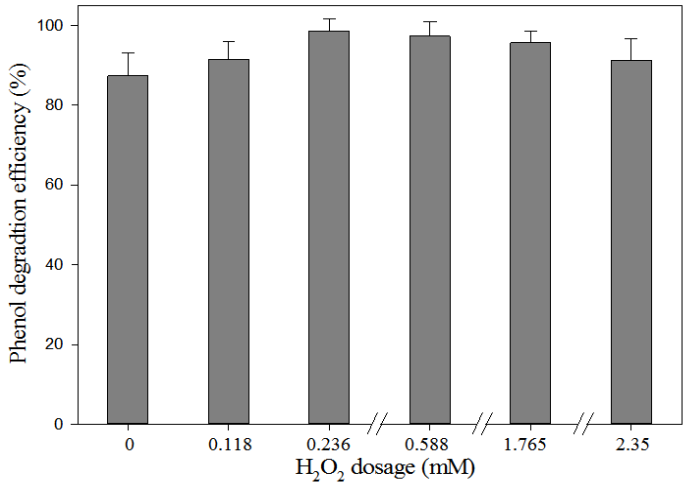

Fig. 9

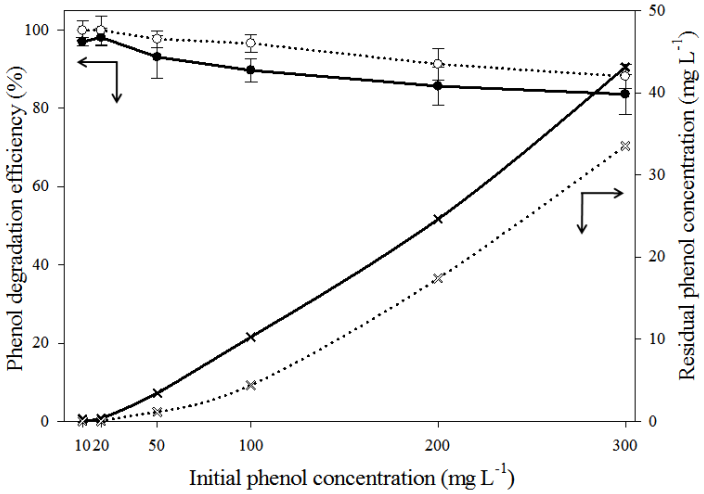

Fig. 10